communications earth & environment

Article

https://doi.org/10.1038/s43247-024-01297-8

Sustained ocean cooling insufficient to reverse sea level rise from Antarctica

Alanna Alevropoulos-Borrill [1] ✉, Nicholas R. Golledge [1], Stephen L. Cornford[2], Daniel P. Lowry [3] & Mario Krapp[3]

Global mean sea level has risen at an accelerating rate in the last decade and will continue to rise for centuries. The Amundsen Sea Embayment in West Antarctica is a critical region for present and future ice loss, however most studies consider only a worst-case future for the region. Here we use ice sheet model sensitivity experiments to investigate the centennial scale implications of short-term periods of enhanced ocean driven sub-ice shelf melting on ice loss and assess what future reduction in melting is necessary to mitigate ice stream retreat and offset global sea level rise. Our findings reveal that restoring elevated melt rates to present-day levels within 100 years causes rates of ice discharge to immediately decline, thereby limiting the overall sea level contribution from the region. However, while ice stream re-advance and slowed ice discharge is possible with reduced basal melting, a centennial scale increase in accumulation must occur to offset the extensive ice loss.

In just the last three decades, the Antarctic ice sheet has contributed 7.4 mm to global sea level rise[1]. While the future of the ice sheet remains uncertain[2], the rate of ice loss from the continent is increasing[3]. As the atmosphere and oceans continue to warm due to rising global emissions, the ice sheet edges closer to an unknown critical threshold for future unstable retreat[4,5]. Worst-case ice sheet futures are often projected[5], but in spite of present warming trends, there remains an opportunity to actively mitigate future climate change[1] and prevent future ice sheet runaway retreat[6]. Plausible scenarios exist where the rate of Antarctic sea-level contribution can be slowed through reduced emissions[6], targeted geoengineering[7] or as a result of climate variability[8]. Here we investigate future scenarios whereby Antarctica ice loss could be limited.

The Amundsen Sea Embayment (ASE, Fig. 1a, b) in West Antarctica dominates ice mass loss from the Antarctic continent[3]. In this sector, ice discharge into the ocean is accelerating due to reductions in resistive stresses caused by ocean-driven ice shelf melting[9,10]. The region is in a state of disequilibrium, as increasing ice discharge across grounding lines and associated high ice shelf melt rates are not matched by mass gain through accumulation[11]. Accelerated ice loss from the ASE is projected in response to local subsurface ocean warming as a result of increasing anthropogenic emissions[12]. Continual increases in ASE sub-ice shelf melt rates could initiate unstable retreat and collapse of the sector[13], as early as 2300[14]. As a climate-sensitive tipping point, this sector provides a regional case study for exploring the conditions required to prevent runaway ice sheet retreat[14,15].

Increasing ice discharge in the ASE is driven by high sub-ice shelf melt rates, which occur when warm circumpolar deep water (CDW) floods the continental shelf and accesses ice shelf cavities[11]. While CDW is blocked from much of the Antarctic continent due to a deepened thermocline and shallow bathymetry, the warm water infiltrates the continental shelf when the thermocline shoals above the depth of troughs that intersect the shelf[16–18]. These deep bathymetric troughs provide channels that subsequently deliver CDW toward grounding lines, driving high melt rates[17,19,20]. Observations and modelling show that the onshore transport of CDW is increasing in response to the strengthening of westerly winds[16], although decadal oscillations in far-field temperature[21–23] and changes to the strength and position of local synoptic systems[24–26] introduce variability to the trend. While the future climatology of the ASE is uncertain, it is widely accepted that future changes in the volume of CDW within ASE ice shelf cavities will dictate future mass loss[12,27,28].

Given observed trends of mass change in the ASE, ice sheet modelling studies often focus on the upper-end of projected mass loss[29–31], and worst-case scenarios receive much attention[5,32]. However, cool ocean conditions and reduced sub-ice shelf melt rates could occur if CDW were to be blocked from ice self cavities, limiting the direct forcing of the ice sheet. Climatologically driven variability in the thermocline depth over decadal timescales[33] causes multi-year periods of cool ocean conditions that coincide with stagnated ice sheet retreat[8]. Specifically, a negative southern annular mode (SAM) and La Niña conditions cause reduced CDW upwelling into the region, which promotes ice stream deceleration[8]. While direct observations over the last 30 years show only multi-year cool periods, a shift or reversal in the climatological regime to a persistent negative SAM could

[1]Antarctic Research Centre, Victoria University of Wellington, Wellington, New Zealand. [2]Centre for Polar Observation and Modelling, University of Bristol, Bristol, UK. [3]GNS Science, Lower Hutt, New Zealand. ✉e-mail: alanna.alevropoulosborrill@vuw.ac.nz

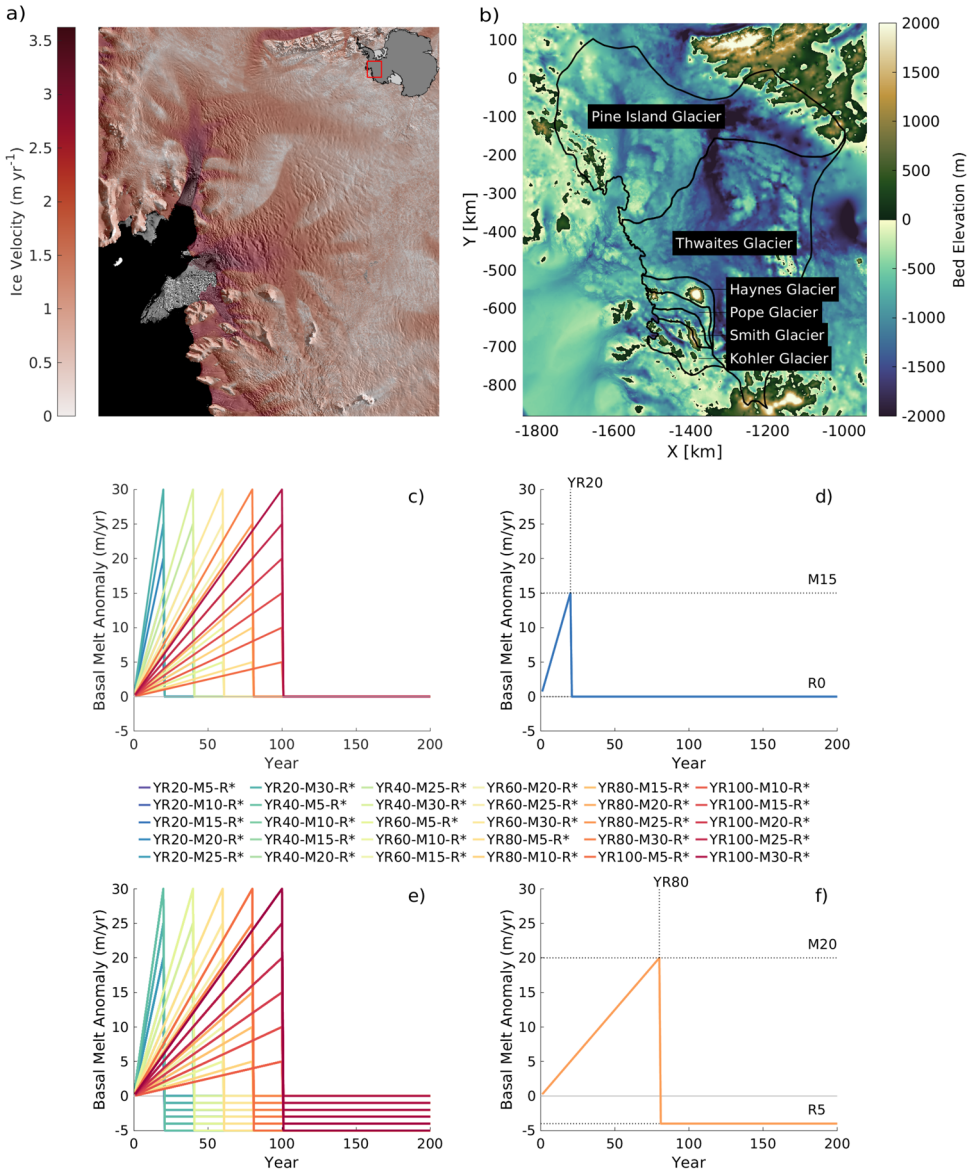

Fig. 1 | Amundsen Sea Embayment domain and ensemble of prescribed melt rate anomalies. a Amundsen Sea Embayment surface velocity[47] overlain on MODIS satellite imagery of the region created using the Antarctic Mapping Tools MATLAB package[53]. **b** Amundsen Sea Embayment bed elevation[40] with labelled and outlined ice stream basins[47]. **c–f** Description of ice sheet model simulation melt rate forcings for the unfiltered ensemble. **c** Time-varying sub-ice shelf melt rate anomalies for the restored melt simulations (R0). The 30 melt anomaly forcings are varied for 5 fixed time periods to 6 different magnitudes before being reduced to the present day. **d** Example of the YR20–M15–R0 forcing where the melt rate anomaly is linearly increased to 15 m y^{-1} over 20 years before being reduced to zero (R0). **e** Ensemble 180 time-varying melt rate anomalies, which include reduced melt rates relative to the present day. The R-value describes the magnitude of anomaly reduction ranging from zero to five. The R* label accounts for all reduction (*R*) values. **f** Example of the YR80–M20–R4 simulation forcing. Dotted lines are used to emphasise the YR, M and R numbers in the simulation codes.

restore ocean conditions to a cooler state[16], although current warming trends and modelled projections give no indication of such an event occurring over coming centuries[12]. Cooler ocean conditions could alternatively be promoted through the physical blocking of CDW by an artificial submarine wall[34]. Such a geoengineering solution could cool and freshen water masses interacting with the two major ASE glaciers[35]. While plausible, the effects of future cool-ocean periods on ice sheet mass loss from the ASE are rarely considered.

Here, ice sheet model sensitivity experiments are used to explore the impacts of multi-decadal periods of idealised ocean forcing on mass loss in the ASE and explore the conditions required to reverse mass loss trends and re-advance grounding lines. Simulations are initially forced with increases in sub-ice shelf melt rates over prescribed durations to explore the centennial scale impacts of multi-decadal periods of increased climate forcing. These simulations are then extended to include reduced melt rates following varied periods of retreat, which replicate local ocean cooling that could hypothetically occur from climate variability[21], cooling from aggressive climate change mitigation strategies, or CDW blocking through local geoengineering[35]. The purpose of these experiments is to better understand how ASE ice streams respond to varied periods of increased melting and to explore whether reduced melting can offset or prevent the unstable retreat of the ASE and re-advance grounding lines.

Results

We present an ensemble of 200-year-long ice sheet model simulations (Fig. 2a, b) forced with perturbed sub-ice shelf (henceforth basal) melting (Fig. 1c, d). The 120 observationally consistent simulations selected for further analysis are comprised of 6 groups of 20 (Fig. 1d). For the initial 20 validated simulations, basal melt rates are increased over different durations and then returned to present-day levels to demonstrate the committed ice sheet contribution to periods of perturbed melt rates (Fig. 1c, d). For the 5 additional groups, we explore mitigated ice loss scenarios whereby a constant negative melt rate anomaly between 1 and 5 m y^{-1} is applied to represent cooler ocean conditions following the fixed periods of increased melting (Fig. 1e, f). The simulation codes relate to the duration of forcing (YR in years), the magnitude of the maximum forcing (M in m y^{-1}) and the magnitude of reduction (R in m y^{-1}) where R0 simulations are reduced to present-day basal melt rates. We compare simulations with a control of constant present-day forcing over 200 years.

The simulations are presented as the 'restored' and 'reduced' melt simulations, where the former sees basal melt rates restored to the present

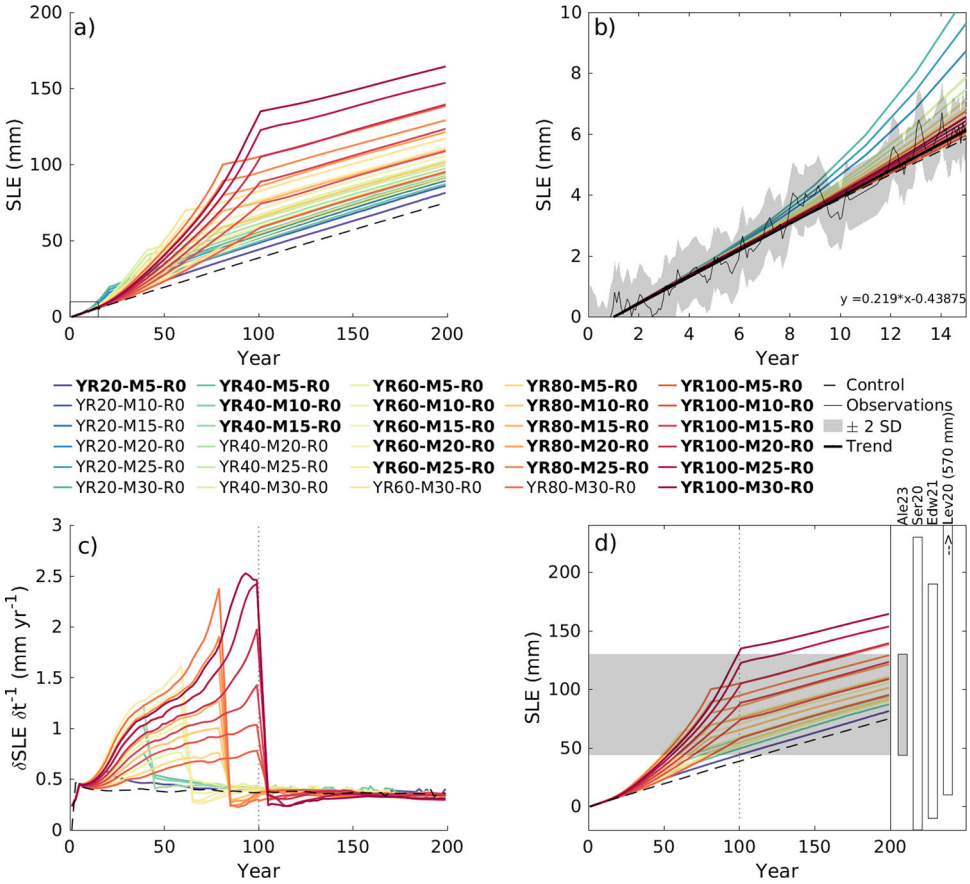

Fig. 2 | Time evolving mass loss for restored melt simulations. a Projected 200-year sea level equivalent (SLE) for all unfiltered 30 R0 simulations and the control. The black line and shading within the inset box show the observations of Antarctic mass loss as a sea level equivalent from gravity recovery and climate experiment (GRACE) Antarctica data from 2007 to 2022. **b** Enlarged inset from **a** with the addition of an equation describing the observational trend. **c** Rate of sea level contribution for the R0 subgroup and control simulation. The dotted vertical line marks the model year 100. **d** Projected 200-year sea level equivalent from a subset of the R0 simulations that are consistent with observations and the control simulation. The grey region shows the range of SLE for all subgroup members in the model year equivalent to 2100. The dotted vertical line marks the simulation year 100. Boxes show the 2100 SLE ranges using SSP1–26 and SSP5–85 from existing studies: this study Alev23, Ser20[2], Edw21[37] and Lev20[36]. The subset of simulations that are consistent with observations have bold label names in the legend.

day (R0; Fig. 1c), the latter reduced further (R1–5; Fig. 1e). Where used, 'R*' describes all R values (e.g. R0–5).

Restored melt simulations

The R0 simulations capture the future centennial scale response of the ASE ice streams to multi-decadal climate forcing periods (Fig. 2c). The sea level equivalent (SLE) contribution from ice stream discharge therefore describes the committed mass loss from fixed periods of increased basal melt anomalies. After 100 years, the ASE mass loss range is equivalent to 44 to 130 mm of global sea level equivalent (Fig. 2d), which lies within the range of projections from existing studies[2,36,37]. In all simulations, the mass loss increases for the following 100 years despite the reduction in melt rates to present-day, resulting in an end-of-simulation mass loss range of 82–165 mm SLE (Fig. 2d).

For each simulation, once the melt rate is reduced to present-day values, the rate of mass loss declines to below the control simulation (Fig. 2c). The simulations with the greatest cumulative total melting experience the lowest ongoing rate of mass loss (Fig. 2c), indicating that high-end simulations are most sensitive to reduced basal melting. Removing the melting anomaly and reducing melting to present-day causes an immediate reduction in the rates of mass loss, reiterating the direct sensitivity of mass change and ice sheet discharge to basal melt rates.

After 100 years, there is a widespread in the grounding line positions across the group of simulations (Fig. 3a–c). The 14,494 km^2 difference in the area of retreat between the lowest and highest forced simulations is dictated by differences in the cumulative, total melt over the period. Retreat remains minimal for the low-end simulation at Pine Island Glacier and Pope Smith and Kohler Glaciers, whilst up to 45 km of retreat occurs in the eastern trunk of Thwaites Glacier (Fig. 3a).

During the second century, the range in the grounded area reduces as grounding lines dynamically migrate toward similar topographically controlled positions in the absence of additional melting (Fig. 3c). For simulations with the greatest total melt, the grounding line of Pine Island Glacier advances 1839 km^2 over the second century along the main trunk. Similarly, the Pope Smith and Kohler glaciers experience re-grounding and advance of 640 km^2 (Fig. 3c, d). The end of simulation grounding line positions for Thwaites Glacier remains retreated. Over the second century, the high-end simulations experienced minimal change in grounding line position, with some retreat balanced by the advance of Pine Island, Pope Smith and Kohler Glaciers. In contrast, simulations with lower melting experience continued dynamic retreat in the absence of additional melting.

The relationship between the end of simulation cumulative melt and SLE varies for each drainage basin due to differences in ice stream dynamics. The dependence of grounded area change on melt for Pine Island, Pope, Smith and Kohler Glaciers are the same. However, the behaviour of mass change for the two basins differs. Although Pope Smith and Kohler show the greatest range in cumulative melt across the subset of simulations due to the differences in ice shelf area extent, the drainage basin has the lowest SLE. The minimum SLE contribution over 200 years from Pope Smith and Kohler Glaciers is 10 mm compared with 30 mm from Pine Island Glacier (Fig. 3f), where the latter has a larger total ice volume. In contrast, Thwaites Glacier shows the greatest extent of mass loss, reaching 70 mm SLE by the end of the simulation despite experiencing lower cumulative melt. Both the sensitivity to melting and the committed mass loss differ for each basin due to their differences in geometry and initial state.

Reduced melt simulations

To quantify the reduction in melt rates required for ice stream re-advance and mitigated future mass loss, we consider a range of melt rate reductions below present-day. Reductions in the melt rate anomaly lead to the advance of ice stream grounding lines (Fig. 4b) and lower total mass loss over 200 years from the ASE in all simulations relative to the restored melt

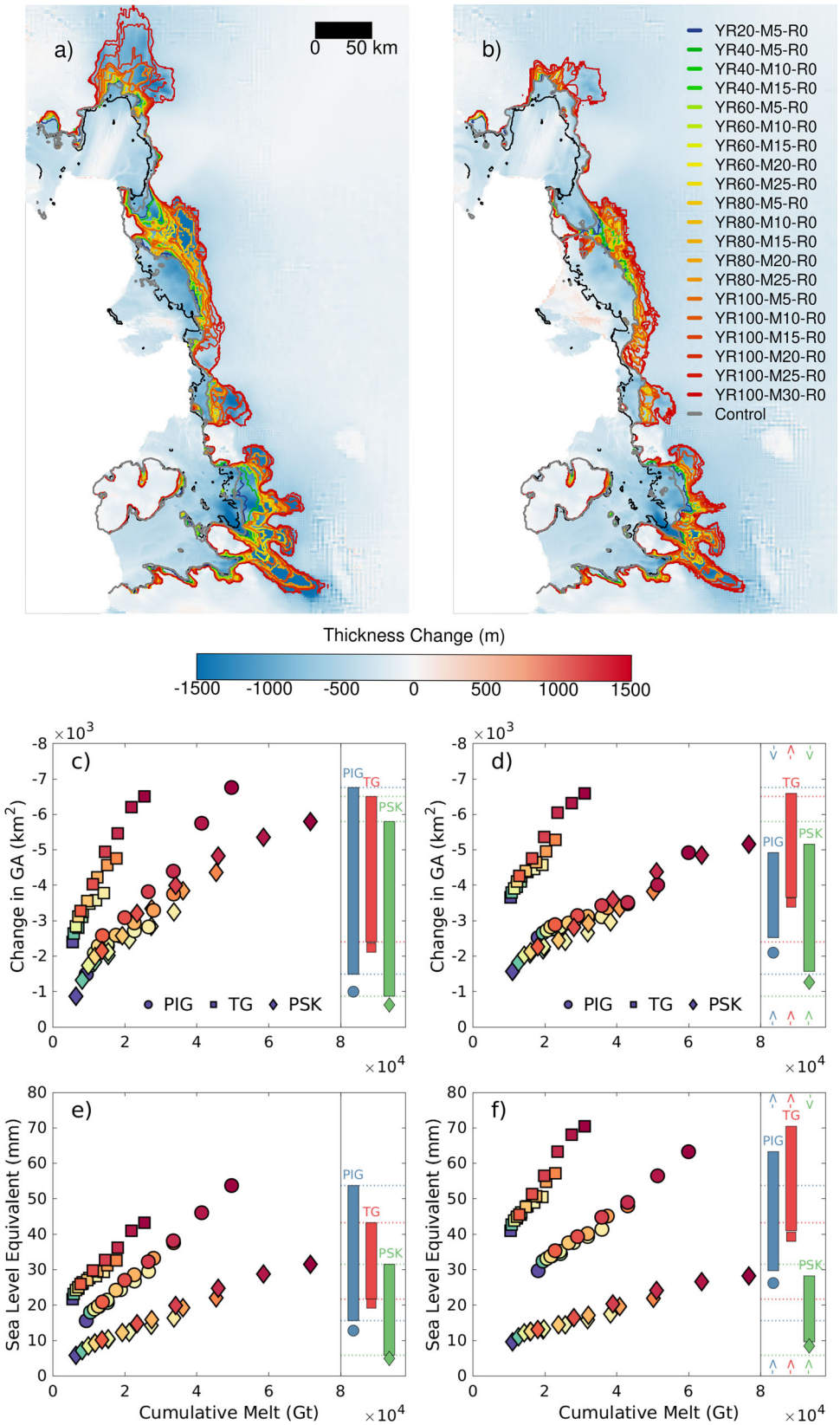

Fig. 3 | Grounded area and sea level equivalent snapshots. a, **b** Map of grounding line positions for each simulation in the restored melt subset (R0) plotted at different time snapshots **a** Year 100, **b** Year 200. Each line represents a different simulation in the subset which is colour-coded with respect to the forcings in Fig. 1a. The background of the map shows the thickness change for the snapshot year in the high-end simulation (YR100–M30) relative to the control. **c**, **d** Scatter plot of change in the grounded area (GA) for each drainage basin for the snapshot year plotted against the respective cumulative sub-ice shelf melt for the same year. Here, negative GA values describe retreat. Each point represents the values for a different simulation in the subset. Panels show years **c** 100 **d** 200. Bar plots to the right of each panel show the range between the lowest and highest change in grounded area for each ice stream within the subset of simulations for the particular snapshot year. Coloured dotted lines show basin change in GA for the high-end simulation in the year 100 for both (**c**) and (**d**). Arrows in **d** show the direction of change of the low and high ends of the variable between years 100 and 200. **e**, **f** Same as **c**, **d** but for sea level equivalent contribution.

simulations (R0; Fig. 4a). Greater reduction in melt rates are associated with a higher number of simulations with lower SLE than the control by the year 200 (Fig. 4a). A melt reduction of 2 m y^{-2} below present-day (R2) is required to prevent any ongoing mass loss for the YR100–M30 high-end simulation, reducing the rate of SLE contribution to approximately 0 mm y^{-1} (Fig. 4e). Further, reducing melt rates from 0 to 5 m y^{-1} below present-day lowers the upper-end SLE contribution by 60 mm, from 165 to 105 mm (Fig. 4a).

The ice loss response of the ASE to melt reduction depends on the prior melting history. This can be seen from the distribution of simulations in each R group, where the increased R value represents a reduction in the

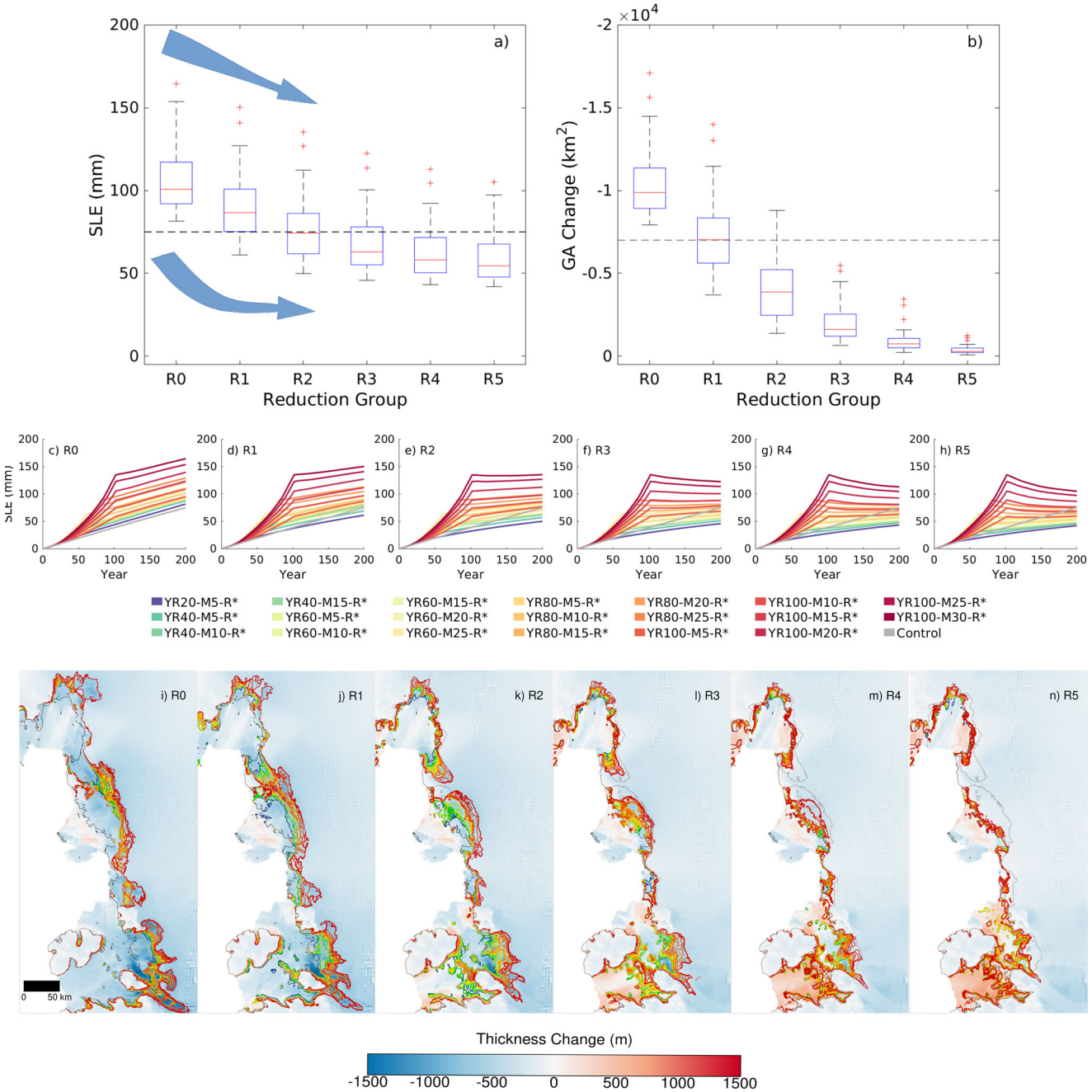

Fig. 4 | Whole ensemble grounded area change and mass loss. a Box plots of the year 200 sea level equivalent for each R group of simulations, the dotted line is the control. Blue arrows illustrate the trend in upper and lower bounds, as discussed in the text. Box plots incorporate all 180 simulations, including those filtered from the ensemble, in order to have a normal distribution. **b** Box plots of year 200 grounded area change (where negative values describe retreat) for each R group of simulations, dotted line is the control. **c**–**h** Sea level equivalent contribution time series for each simulation where each subplot shows each group of reduced melt (R0–R5). **i**–**n** Grounding line position in the year 200 for each simulation within each group of melt rate reductions (R). Each panel represents a different reduction group. The background colour for each panel depicts the end of simulation thickness change for the highest forced simulation (YR100–M30–R*) in each group.

constant basal melt by an additional 1 m y^{-1} (Fig. 4a). Each 1 m y^{-1} reduction in basal melt anomalies leads to a 7–14 mm reduction in the ensemble maximum SLE. In contrast, there is a minimum committed SLE contribution (Fig. 4a), demonstrated by an asymptotic decrease in the ensemble minimum SLE. Therefore, while the upper end of mass loss can be continuously reduced, there is a limit to which the lower end of SLE can be reduced.

Reduced melt rates promote the re-advance of ASE grounding lines as shown by the positive change in the grounded area (Fig. 4b). As the melt rates are continually reduced, the change in grounded area for all simulations reduces as the grounding lines advance toward their initial positions (Fig. 4i–n). The spread in simulations within each subset of R groups decreases from 83 mm for R0 to 63 mm for R5 (Fig. 4a), where the melt anomaly reduction causes grounding line positions to converge, which counters the effect of the differences in increased melt anomaly (Fig. 4i–n). Unlike the SLE, the R3–R5 reductions result in grounding line positions further downstream than the control due to re-advance (Fig. 4a, b).

Discussion

Short-term increases in sub-ice shelf melt rates have long-term impacts on future sea level rise. In these experiments, limiting ocean-driven enhanced

melting to 20 years compared with 60 years results in a 24 mm lower global sea level contribution over two centuries. This is consistent with DeConto et al.[6], who found that delays in the reduction of melt rates over Antarctica have a long-term influence on sea level[6]. The duration of the forcing period alone is not sufficient to explain the total ice mass loss from simulations in the ensemble. Instead, the end of simulation mass loss is dependent on the total melt over the simulation, which is the combined effect of the duration and magnitude of increased melt rates. Short-term periods of large increases in melting can therefore have the same long-term sea level effect as longer periods of small increases in melting.

Restoring basal melting to present-day after <100 years of enhanced melting results in an immediate reduction in the rate of mass loss from the ASE (Fig. 2d). The reduced melt rates promote re-advance of Pine Island, Haynes, Pope, Smith and Kohler Glacier grounding lines and pauses the further retreat of Thwaites Glacier in the high-end simulations (Fig. 3). The immediate reduction in the rate of ice discharge and resulting sea level contribution is indicative that the ice streams reach a point of transient stability as rates of grounding line retreat are slowed[4], which is consistent with the findings of Hill et al.[15] who perturbed melt rates over a fixed 20 years period and found restored thickness and advance. That being said, while rates of mass loss can be reduced, and the upper end of sea level contribution lowered, rates of mass loss remain positive, and therefore the region continues to contribute to sea level rise (Fig. 2d). Instead, reduced melt rates below present-day are required to offset the increased mass loss that occurs in response to periods of enhanced melting.

The mitigated future change scenarios show that total mass loss from the ASE can be limited through reduced melt rates. Reducing present-day melt rates by 1 m y^{-1} lowers the upper and lower end of SLE by 14–20 mm, respectively (Fig. 4a). Lowered melt rates lessen the ice shelf thinning rates and promote dynamic thickening leading to increased buttressing[9,10]. In this scenario, reduced melt rates lead to ice stream deceleration which reduces ice discharge (Supplementary Figs. 1 and 2). Local thickening through deceleration results in grounding line re-advance which increases the volume of ice above floatation and therefore reduces the overall sea level contribution. For all simulations with melt rates lowered below present-day, the rate of ongoing mass loss is lower than the control of constant present-day.

Substantially reducing melt rates below present-day for over a century does result in the re-advance of ice stream grounding lines but fails to offset the total ice loss during this time. Reducing melt rates by 5 m y^{-1} following retreat promotes grounding line advance to the near present-day but with a total mass deficit equivalent to 42 to 105 mm of sea level rise over 200 years (Fig. 4a). Total ice mass loss and grounding line position are therefore independent. While dynamic thickening occurs around the grounding line to drive the advance, this again does not offset the widespread thinning that occurs over the entire catchment during the 200-year simulations (Fig. 3), which would leave the region more susceptible to future climate-forced retreat. In these simulations, the constant prescribed snow accumulation over grounded ice offsets ~0.7 mm y^{-1} of SLE, which is accounted for in the SLE contribution. Therefore a 60% increase in accumulation over grounded ice for a minimum of 176 years is required to entirely offset sea level contribution from the low-end simulation with a melt rate reduction of 5 m y^{-1} (YR20–M5–R0, Supplementary Fig. 3). Although grounding line re-advance in these scenarios is encouraging, grounding line position should not be used as the sole indicator of ice stream health.

The majority of mass loss and retreat occurs in the Thwaites Glacier Basin, which has a complex response to the forcing (Fig. 3d, f). The large, fast flowing[38], ice stream experiences the greatest committed mass loss of 40 mm in response to constant present-day melting. Thwaites Glacier also shows the greatest sensitivity to melting. Although the present geometry of the ice shelf provides limited buttressing resistance to upstream ice[39], our simulations instead show a high sensitivity to increased melting. This can be explained by the increases in buttressing as a result of the evolving geometry of the ice shelf (Supplementary Figs. 4 and 5). In response to reduced melt rates, the rate of ice discharge immediately slows and continued grounding line retreat is limited. During the second century, in the absence of additional melting, the low cumulative forced simulations experience continued retreat leading to a clustering of the end of simulation grounding lines around two topographic ridges[40,41], indicative of marine ice sheet instability[4]. Although the second-century retreat is slowed in high forced simulations (Fig. 3a, b), that is not to say ongoing unstable retreat has not been triggered during this period.

In the reduced melt, the rate of ongoing mass loss is dependent on the prior melting history. Simulations with the greatest cumulative forcing during the initial forcing period result in the lowest ongoing rate of mass loss, which is seen as mass gain in some scenarios. These high melt simulations respond to melt by accelerating and retreating, which coincides with a lowering of surface slope around the grounding line (Supplementary Figs. 1 and 2). As the melt rates are reduced, the simulations with the highest perturbed velocities result in a greater rate of dynamic thickening of the ice shelves (Supplementary Figs. 1 and 2). This process provides increased buttressing of ice streams in addition to lowered driving force and reduced ongoing ice discharge due to the flattened surface slope. The greater the reduction in melting, the more amplified this effect becomes (Supplementary Figs. 1 and 2). This effect is most notable for Pine Island, Pope Smith and Kohler Glaciers and therefore dominates the overall mass trend (Supplementary Fig. 6). Reduced melting therefore has the greatest impact on upper-end projections and results in the largest mass loss mitigation effect.

In this research, we investigate the ocean conditions required to limit mass loss from the Amundsen Sea Embayment ice streams. We find that short periods of high increases in sub-ice shelf melting have comparable sea level rise outcomes to long periods of low increases. As total melt dictates total mass loss from the region, minimising ocean-driven melting through reduced emissions or geoengineering is essential for preventing serious future sea level rise. Reduced melt rates below present-day can significantly limit ongoing retreat and promote the re-advance of grounding lines within two centuries. Reducing melt rates by up to 5 m y^{-1} below present levels promotes ice stream re-advance to present-day positions, despite extensive prior retreat, but inland thickening from substantially increased accumulation will also be necessary to reverse Antarctica's contribution to future sea level rise.

Methods

Ice sheet model

The BISICLES ice sheet model is used to perform the described simulations[42]. The ice sheet model solves one-layer longitudinal stress balance approximation in two dimensions (L1L2)[43]. The model has adaptive mesh refinement capabilities, which are employed throughout this investigation. Here, there are 4 levels of refinement, from 4 km coarsest to 0.25 km finest resolution. The mesh evolves through time with the finest mesh level closest to the grounding line. For more detail refer to Cornford et al.[42,44]. Grounding lines are explicitly determined at the transition between grounded and floating grid cells, here, no additional grounding line scheme is required due to the fine horizontal resolution of the grid.

Model configuration

Simulations are performed for a regional ASE domain with topography and thickness derived from BedMachine version 1[40]. The surface mass balance field (SMB) from Arthern et al.[45] is held constant in order to focus on the ocean-forced response of the region. A three-dimensional internal ice temperature field produced by Pattyn et al.[46] is applied, which does not evolve through time. Basal traction and ice viscosity coefficients are determined through an inverse procedure so that the initial modelled velocities are consistent with observations for 2013–2016[44,47]. We use the Weertman sliding law with a coefficient of $m = \frac{1}{3}$[48]. We apply a fixed calving front and impose a minimum ice thickness of 10 m. Melt rates are applied only to fully floating grid cells.

Drainage basins

We present the results by grouping ice streams according to their drainage basin. The Pine Island and Thwaites Glacier basins remain separate, and their boundaries are shown in Fig. 1b. The Pope, Smith and Kohler Glaciers (PSK) basin described in this study is made up of the three small ice streams that feed into the Dotson and Crosson ice shelves, their boundaries are shown in Fig. 1b. Haynes Glacier as an individual drainage basin is not considered.

Ensemble description

We perform a 181-member ensemble consisting of 180 regional ASE (Fig. 1a, b) ice sheet model simulations forced with perturbed sub-ice shelf basal melting and a control simulation with constant present-day basal melting[44,49] (Fig. 1c, d). The 180 forced simulations are comprised of 6 groups of 30. Each group of 30 simulations is forced with increased melt rate anomalies over 5 fixed durations from 20 to 100 years, which are each increased linearly to 6 different magnitudes ranging from 5–30 m y^{-1}.

For the initial 30 simulations, basal melt rates are returned to present-day values upon removal of the anomaly (R0) (Fig. 1c, d). In this group, the high and low-end simulations are YR100–M30 and YR20–M5, respectively, where 30 (or 5) indicates the basal melt rate after 100 (or 20) years. For the 5 additional groups, a constant negative melt rate anomaly is applied (Fig. 1e, f). The magnitude of the negative anomaly ranges between 0 and 5 m y^{-1} for each of the 6 groups.

Sub-ice shelf melting

An initial steady-state basal melt rate field produced by Cornford et al.[44] is applied to replicate present-day melt rates over the ASE. This product was tuned to reproduce observed ice shelf thinning rates when accounting for ice flux divergence[49]. It has been further smoothed and scaled with the highest melt rates concentrated at the grounding line, which decreases toward the ice front (see ref. [49] for more detail). The melt field is updated at every time step to extend concentrated melting to newly un-grounded ice where the grounding line retreats. In all forced simulations, anomalies are added to this background field. Anomalies are scaled according to observed patterns of basal melting, where the highest melting is concentrated at the grounding line[29,49,50]. Anomalies remain concentrated at the grounding line as it migrates.

To explore the effects of local ocean cooling, we apply melt rate reduction anomalies of up to 5 m y^{-1}. Sub-ice shelf melt rates are shown to depend quadratically on far-field mid-depth temperatures[33]. In the Amundsen Sea Embayment, the sensitivity of basal melt to thermal driving (the temperature above the local freezing point), for a baseline present-day temperature of 1.65 °C, varies from 10 to 19 m y^{-1} $°C^{-1}$ [33]. According to Naughten et al.[16], mid-depth ocean temperature variability over the historical period (20th century) varied by up to 0.4 °C, equating to 4–7.6 m y^{-1} of natural melt rate variability beneath ice shelves. Subsequently, melt rate reductions up to 5 m y^{-1} applied here lie within the range of observed variability in the region. The same melt rate reduction values have been used to determine sub-ice shelf melt forcing in other ice sheet modelling studies[15,51].

Ensemble filtering

The 180-member ensemble is filtered to remove simulations where the rate of mass loss is inconsistent with the present-day trend over 2007–2022, based on GRACE satellite-derived observational data of Antarctic mass loss[52] (Fig. 2a, b). During comparison, we assume a present-day model state representative of 2007 and therefore compare model years 0–15 with observations. Antarctic mass loss between 2007 and 2022 is extracted and converted to global sea level equivalent assuming an ocean density of 1027 kg m^{-3}, an ice density of 917 kg m^{-3} and a global ocean area of 3.618×10^8 km^2. The de-trended standard deviation of the observational data is used to provide a two-standard deviation uncertainty interval over the time series. Simulations with a trend of sea level equivalent consistent with observations over the corresponding years are identified and selected for further investigation.

Data availability

Ice sheet model input fields and simulation outputs are available on the Open Science Framework (https://osf.io/uyma6/).

Code availability

BISICLES is freely available as open-source code from https://commons.lbl.gov/display/bisicles/BISICLES.

Received: 25 July 2023; Accepted: 29 February 2024;
Published online: 02 April 2024

References

1. Lee, J.-Y. et al. Future global climate: Scenario-based projections and near-term information. In Masson-Delmotte, V. et al. (eds.) *Climate Change 2021: The Physical Science Basis. Contribution of Working Group I to the Sixth Assessment Report of the Intergovernmental Panel on Climate Change*, book section 4 (Cambridge University Press, Cambridge, UK and New York, NY, USA, 2021). https://www.ipcc.ch/report/ar6/wg1/downloads/report/IPCC_AR6_WGI_Chapter04.pdf.
2. Seroussi, H. et al. ISMIP6 Antarctica: a multi-model ensemble of the Antarctic ice sheet evolution over the 21st century. *Cryosphere* **14**, 3033–3070 (2020).
3. Rignot, E. et al. Four decades of Antarctic Ice Sheet mass balance from 1979–2017. *Proc. Natl Acad. Sci. USA* **116**, 1095–1103 (2019).
4. Schoof, C. Ice sheet grounding line dynamics: Steady states, stability, and hysteresis. *J. Geophys. Res.* **112**, F03S28 (2007).
5. DeConto, R. & Pollard, D. Contribution of Antarctica to past and future sea-level rise. *Nature* **531**, 591–597 (2016).
6. DeConto, R. M. et al. The paris climate agreement and future sea-level rise from antarctica. *Nature* **593**, 83–89 (2021).
7. Moore, J. C. et al. Targeted geoengineering: local interventions with global implications. *Glob. Policy* **12**, 108–118 (2021).
8. Dutrieux, P. et al. Strong sensitivity of Pine Island ice-shelf melting to climatic variability. *Science* **343**, 174–178 (2014).
9. Gudmundsson, G. H. Ice-shelf buttressing and the stability of marine ice sheets. *Cryosphere* **7**, 647–655 (2013).
10. Fürst, J. J. et al. The safety band of Antarctic ice shelves. *Nat. Clim. Change* **6**, 479–482 (2016).
11. Smith, B. et al. Pervasive ice sheet mass loss reflects competing ocean and atmosphere processes. *Science* **368**, 1239–1242 (2020).
12. Naughten, K. A. et al. Future projections of Antarctic Ice Shelf melting based on CMIP5 scenarios. *J. Clim.* **31**, 5243–5261 (2018).
13. Schoof, C. Marine ice sheet stability. *J. Fluid Mech.* **698**, 62–72 (2012).
14. Reese, R. et al. The stability of present-day antarctic grounding lines–part 2: onset of irreversible retreat of amundsen sea glaciers under current climate on centennial timescales cannot be excluded. *Cryosphere* **17**, 3761–3783 (2023).
15. Hill, E. A. et al. The stability of present-day antarctic grounding lines–part 1: no indication of marine ice sheet instability in the current geometry. *Cryosphere* **17**, 3739–3759 (2023).
16. Naughten, K. A. et al. Simulated twentieth-century ocean warming in the Amundsen Sea, West Antarctica. *Geophys. Res. Lett.* **49**, e94566 (2022).
17. Nakayama, Y., Timmermann, R., Rodehacke, C. B., Schröder, M. & Hellmer, H. H. Modeling the spreading of glacial meltwater from the Amundsen and Bellingshausen Seas. *Geophys. Res. Lett.* **41**, 7942–7949 (2014).
18. Holland, P. R., Bracegirdle, T. J., Dutrieux, P., Jenkins, A. & Steig, E. J. West Antarctic ice loss influenced by internal climate variability and anthropogenic forcing. *Nat. Geosci.* **12**, 718–724 (2019).

19. Wåhlin, A. et al. Variability of warm deep water inflow in a submarine trough on the Amundsen Sea shelf. *J. Phys. Oceanogr.* **43**, 2054–2070 (2013).
20. Deb, P. et al. Summer drivers of atmospheric variability affecting ice shelf thinning in the Amundsen Sea Embayment, West Antarctica. *Geophys. Res. Lett.* **45**, 4124–4133 (2018).
21. Jenkins, A. et al. Decadal ocean forcing and Antarctic ice sheet response: Lessons from the Amundsen Sea. *Oceanography* **29**, 106–117 (2016).
22. Steig, E. J., Ding, Q., Battisti, D. & Jenkins, A. Tropical forcing of Circumpolar Deep Water inflow and outlet glacier thinning in the Amundsen Sea Embayment, West Antarctica. *Ann. Glaciol.* **53**, 19–28 (2012).
23. Paolo, F. et al. Response of Pacific-sector Antarctic ice shelves to the El Niño/Southern oscillation. *Nat. Geosci.* **11**, 121–126 (2018).
24. Assmann, K. et al. Variability of Circumpolar Deep Water transport onto the Amundsen Sea Continental shelf through a shelf break trough. *J. Geophys. Res.* **118**, 6603–6620 (2013).
25. Dotto, T. S. et al. Control of the oceanic heat content of the Getz-Dotson Trough, Antarctica, by the Amundsen Sea Low. *J. Geophys. Res.* **125**, e2020JC016113 (2020).
26. Hosking, J. S., Orr, A., Bracegirdle, T. J. & Turner, J. Future circulation changes off West Antarctica: Sensitivity of the Amundsen Sea Low to projected anthropogenic forcing. *Geophys. Res. Lett.* **43**, 367–376 (2016).
27. Turner, J. et al. Atmosphere-ocean-ice interactions in the Amundsen Sea embayment, West Antarctica. *Rev. Geophys.* **55**, 235–276 (2017).
28. Donat-Magnin, M. et al. Ice-shelf melt response to changing winds and glacier dynamics in the Amundsen Sea Sector, Antarctica. *J. Geophys. Res.* **122**, 10206–10224 (2017).
29. Alevropoulos-Borrill, A., Nias, I., Payne, A. J., Golledge, N. R. & Bingham, R. J. Ocean forced evolution of the Amundsen Sea catchment, West Antarctica, by 2100. *Cryosphere* **14**, 1245–1258 (2020).
30. Robel, A. A., Seroussi, H. & Roe, G. H. Marine ice sheet instability amplifies and skews uncertainty in projections of future sea-level rise. *Proc. Natl Acad. Sci. USA* **116**, 14887–14892 (2019).
31. Nias, I. J., Cornford, S. L., Edwards, T. L., Gourmelen, N. & Payne, A. J. Assessing uncertainty in the dynamical ice response to ocean warming in the Amundsen Sea Embayment, West Antarctica. *Geophys. Res. Lett.* **46**, 11253–11260 (2019).
32. Martin, D. F., Cornford, S. L. & Payne, A. J. Millennial-scale vulnerability of the Antarctic Ice Sheet to regional ice shelf collapse. *Geophys. Res. Lett.* **46**, 1467–1475 (2019).
33. Jenkins, A. et al. West Antarctic Ice Sheet retreat in the Amundsen Sea driven by decadal oceanic variability. *Nat. Geosci.* **11**, 733–738 (2018).
34. Moore, J. C., Gladstone, R., Zwinger, T. & Wolovick, M. Geoengineer polar glaciers to slow sea-level rise. *Nature* **555**, 303–305 (2018).
35. Gürses, O., Kolatschek, V., Wang, Q. & Rodehacke, C. B. Brief communication: a submarine wall protecting the Amundsen Sea intensifies melting of neighboring ice shelves. *Cryosphere* **13**, 2317–2324 (2019).
36. Levermann, A. et al. Projecting Antarctica's contribution to future sea level rise from basal ice-shelf melt using linear response functions of 16 ice sheet models (LARMIP-2). *Earth Syst. Dyn. Discuss.* **2019**, 1–63 (2019).
37. Edwards, T. L. et al. Projected land ice contributions to twenty-first-century sea level rise. *Nature* **593**, 74–82 (2021).
38. Milillo, P. et al. Heterogeneous retreat and ice melt of Thwaites Glacier, West Antarctica. *Sci. Adv.* **5**, eaau3433 (2019).
39. Gudmundsson, G., Barnes, J., Goldberg, D. & Morlighem, M. Limited impact of thwaites ice shelf on future ice loss from antarctica. *Geophys. Res. Lett.* **50**, e2023GL102880 (2023).
40. Morlighem, M. et al. Deep glacial troughs and stabilizing ridges unveiled beneath the margins of the Antarctic ice sheet. *Nat. Geosci.* **13**, 132–137 (2020).
41. Castleman, B. A., Schlegel, N.-J., Caron, L., Larour, E. & Khazendar, A. Derivation of bedrock topography measurement requirements for the reduction of uncertainty in ice sheet model projections of Thwaites Glacier. *The Cryosphere.* **16**, 761–778 (2022).
42. Cornford, S. L. et al. Adaptive mesh, finite volume modeling of marine ice sheets. *J. Comput. Phys.* **232**, 529–549 (2013).
43. Schoof, C. & Hindmarsh, R. C. Thin-film flows with wall slip: an asymptotic analysis of higher order glacier flow models. *Q. J. Mech. Appl. Math.* **63**, 73–114 (2010).
44. Cornford, S. et al. Century-scale simulations of the response of the West Antarctic Ice Sheet to a warming climate. *Cryosphere* **9**, 1579–1600 (2015).
45. Arthern, R. J., Winebrenner, D. P. & Vaughan, D. G. Antarctic snow accumulation mapped using polarization of 4.3-cm wavelength microwave emission. *J. Geophys. Res.* **111**, D06107 (2006).
46. Pattyn, F. Antarctic subglacial conditions inferred from a hybrid ice sheet/ice stream model. *Earth Planet. Sci. Lett.* **295**, 451–461 (2010).
47. Mouginot, J., Rignot, E., Scheuchl, B. & Millan, R. Comprehensive annual ice sheet velocity mapping using Landsat-8, Sentinel-1, and RADARSAT-2 data. *Remote Sens.* **9**, 364 (2017).
48. Weertman, J. On the sliding of glaciers. *J. Glaciol.* **3**, 33–38 (1957).
49. Nias, I. J., Cornford, S. L. & Payne, A. J. Contrasting the modelled sensitivity of the Amundsen Sea Embayment ice streams. *J. Glaciol.* **62**, 552–562 (2016).
50. Rignot, E., Jacobs, S., Mouginot, J. & Scheuchl, B. Ice-shelf melting around Antarctica. *Science* **341**, 266–270 (2013).
51. Reese, R., Albrecht, T., Mengel, M., Asay-Davis, X. & Winkelmann, R. Antarctic sub-shelf melt rates via PICO. *Cryosphere* **12**, 1969–1985 (2018).
52. Wiese, D., Yuan, D.-N., Boening, C., Landerer, F. & MM, W. JPL GRACE and GRACE-FO Mascon Ocean, Ice, and Hydrology Equivalent HDR Water Height RL06.1M CRI Filtered Version 3.0, Ver. 3.0, PO.DAAC, CA, USA (2022). Last Accessed 10.03.2023.
53. Greene, C. A., Gwyther, D. E. & Blankenship, D. D. Antarctic mapping tools for MATLAB. *Comput. Geosci.* **104**, 151–157 (2017).

Acknowledgements

The authors thank the two anonymous reviewers for their constructive comments. This work was supported by the Royal Society of New Zealand through contract VUW-1501. We thank the New Zealand Ministry for Business, Innovation and Employment contract ANTA1801 ("Antarctic Science Platform"). The authors wish to acknowledge the use of New Zealand eScience Infrastructure (NeSI) high performance computing facilities and consulting support as part of this research. New Zealand's national facilities are provided by NeSI and funded jointly by NeSI's collaborator institutions and through the Ministry of Business, Innovation & Employment's Research Infrastructure programme. Final thanks go to the BISICLES developers for their ongoing work and technical support.

Author contributions

A.A.-B. and N.R.G. conceived the experiment(s), A.A.-B. conducted the experiment(s) and analysis, S.L.C. provided the initial model state and modelling support. A.A.-B., N.R.G., S.L.C., D.P.L., and M.K. all contributed to the writing of the paper.

Competing interests

The authors declare no competing interests.

Additional information

Supplementary information The online version contains supplementary material available at https://doi.org/10.1038/s43247-024-01297-8.

Correspondence and requests for materials should be addressed to Alanna Alevropoulos-Borrill.

Peer review information *Communications Earth & Environment* thanks the anonymous reviewers for their contribution to the peer review of this work. Primary Handling Editors: Viviane Menezes, Heike Langenberg. A peer review file is available.